

Spectral methods for forward-propagating water waves in conformally-mapped channels

Robert A. Dalrymple, James T. Kirby

Center for Applied Coastal Research, Department of Civil Engineering, University of Delaware, Newark, DE 19716, USA

&

P. A. Martin

Department of Mathematics, University of Manchester, Manchester, UK, M13 9PL

The prediction of wave fields in domains with complicated geometries may be aided by the use of conformal-mapping, which simplifies the shape of the domain. In this conformal domain, parabolic models have been used previously to treat wave problems. In Cartesian coordinates, the angular spectrum model, based on a Fourier transform in the direction perpendicular to the principal propagation direction, has been shown to handle, in principle, a wider range of wave directions than the parabolic model.

Here, the extension of the angular spectrum model to conformally-mapped domains with impermeable lateral boundaries is shown. Next, the Fourier–Galerkin method is developed for conformal domains; this is identical to the angular spectrum model in Cartesian coordinates, but differs in the conformal domain. Finally, a Chebyshev-tau model for conformal domains is developed, based on using Chebyshev polynomials rather than trigonometric functions as a basis. For all models, forward-propagation equations are derived, by splitting the governing elliptic equations into first-order equations. Examples of all methods are shown for a simple conformal mapping that permits the study of waves in a diverging channel and in a circular channel. The forward-propagation models are shown to be optimal for methods that use eigenfunctions for the lateral transform and less accurate for others.

1 INTRODUCTION

Wave modelling in regions where the boundaries are uncomplicated can be easily carried out by a variety of means. For over a decade, parabolic modelling, based on finite-difference methods, has been used with success to examine refraction, diffraction and shoaling of short waves over large coastal areas.^{1–3} More recently, angular spectrum modelling has been used.^{4–7} As originally conceived,⁸ the angular spectrum model involves the decomposition of an incident wave field into plane waves, which are then allowed to propagate into the domain. The resulting wave field is the superposition of these plane waves. This technique is carried out by Fourier transforming the governing equation and initial condition in the lateral direction, and then solving the resulting one-dimensional equations for the Fourier modes, which are then superimposed for the final wave field. This method of expressing the wave field as a Fourier integral or a

trigonometric series has the potential advantage of permitting wider angles of wave approach when compared to parabolic modelling, which is constrained by a preferred propagation direction. Also, the angular spectrum methodology (a review⁹ is available) can be applied to weakly nonlinear water waves,¹⁰ shallow water Boussinesq waves,¹¹ and directional spectra.^{12,13}

For problems that are periodic in one direction, the Fourier trigonometric basis is optimal for the series expansion of the solution in that direction. For other problems, Chebyshev polynomials are usually preferred. For example, Boyd¹⁴ has treated a number of nonlinear wave problems with these polynomials, while Panchang and Kopriva¹⁵ have used them in both horizontal directions in a collocation method for solving the elliptic mild-slope equation. However, the Chebyshev polynomials do not satisfy our lateral boundary conditions, so an equivalent method to the Fourier–Galerkin method will not be possible; a Chebyshev-tau method overcomes this difficulty by using two additional

equations to enforce the boundary conditions and is very similar in application.¹⁶

Wave prediction in realistic coastal situations is often complicated by the layout of breakwaters and other hard structures coupled with variable depths and currents. These complicated situations can often be simplified if a coordinate transformation is used that conforms to the physical boundaries. Hence, we consider a general class of conformal transformations from the Cartesian coordinates (x, y) into boundary-fitted coordinates (u, v) , so that no-flow boundary conditions can be applied on coordinate lines. We then investigate models for forward wave propagation, developed in the transformed domain.

Boundary-fitted coordinates have been used extensively in other fields with good success.^{17,18} In the field of wave propagation, Liu and Boissevain¹⁹ transformed the parabolic model into a non-orthogonal coordinate system to examine the propagation of waves in a diverging channel (harbour entrance). Kirby²⁰ showed that it is important to determine the parabolic model within the mapped domain. Tsay *et al.*²¹ developed some low-order parabolic approximations for several geometries, while Kirby *et al.*²² developed parabolic models for several geometric domains for both small- and large-angle parabolic approximations. They also presented laboratory results for the case of the diverging breakwater.

Here we develop the forward-propagation equations for Fourier–Galerkin, angular spectrum and Chebyshev-tau models in conformal domains, and then compare the results to exact solutions for two simple planforms — waves between diverging breakwaters and waves in a circular channel; these are the same geometries as used before.²² Application to more complicated conformal domains, using numerical codes for the conformal mapping,¹⁸ is straightforward.

2 THEORY: CARTESIAN COORDINATES

The governing equation for the propagation of linear waves in constant water depth is the two-dimensional Helmholtz equation,

$$\frac{\partial^2 \phi}{\partial x^2} + \frac{\partial^2 \phi}{\partial y^2} + k^2 \phi = \nabla^2 \phi + k^2 \phi = 0 \quad (1)$$

where (x, y) are the horizontal Cartesian coordinates and the total wave potential is

$$\text{Re} \left\{ \phi(x, y) \frac{\cosh k(h+z)}{\cosh kh} e^{-i\omega t} \right\}$$

The mean free surface is at $z = 0$ and the bottom is at $z = -h$. The wavenumber k is related to the water depth h and the angular frequency of the wave ω by the dispersion relationship,

$$\omega^2 = gk \tanh kh$$

We are interested in situations in which waves are primarily propagating in the $+x$ direction within a domain of given width. As an example, for a straight channel of width $2b$, with impermeable walls at $y = \pm b$, we can use separation of variables to solve for the velocity potential. Assuming $\phi(x, y) = X(x)Y(y)$, yields two equations

$$X'' + (k^2 - \lambda^2)X = 0 \quad (2)$$

$$Y'' + \lambda^2 Y = 0 \quad (3)$$

For no-flow lateral boundary conditions, we have $Y'(y) = 0$ at $y = \pm b$; therefore we have a Sturm–Liouville problem in the y -direction. The eigenvalues are $\lambda_n = \frac{1}{2}n\pi/b$ and the eigenfunctions are $\{\cos[\lambda_n(y+b)]\}$, $n = 0, 1, 2, \dots$. The corresponding solutions of eqn (2) are exponential functions of x . Finally, summing all the possible solutions together, we obtain

$$\phi(x, y) = \sum_{n=-\infty}^{\infty} a_n \exp \left\{ \pm ix \sqrt{k^2 - \lambda_n^2} \right\} \cos[\lambda_n(y+b)] \quad (4)$$

where the a_n are dimensional constants. The forward-propagating waves will be associated with the positive sign in the exponent. Also, note that for values of $\lambda_n > k$, the forward-propagating wave modes decay exponentially with $+x$.

Another method of solving the two-dimensional eqn (1) is to use a transform in the lateral direction (y), thus reducing it to one-dimensional equations. A general transform pair can be described by

$$\begin{aligned} \Psi_n(x) &= \mathcal{T}_\psi[\phi(x, y)] \\ &= \int_{-b}^b \phi(x, y) \psi_n(y) w(y) dy \quad n = 0, 1, 2, \dots, \end{aligned} \quad (5)$$

$$\begin{aligned} \phi(x, y) &= \mathcal{T}_\psi^{-1}[\Psi(x)] \\ &= \sum_{n=0}^{\infty} \Psi_n(x) \psi_n(y) \quad \text{for } -b < y < b \end{aligned} \quad (6)$$

where $\{\psi_n(y)\}$, $n = 0, 1, 2, \dots$, is a set of functions that are orthogonal (with weight w) over the range $-b \leq y \leq b$, and $\Psi_n(x)$ are the amplitudes of these orthogonal functions. Two common choices for $\psi_n(y)$ are trigonometric functions (Fourier transforms) and Chebyshev polynomials.

To proceed, we transform eqn (1) into a set of equations for the amplitudes:

$$\begin{aligned} \frac{d^2 \Psi_n(x)}{dx^2} + \mathcal{T}_\psi \left[\frac{\partial^2 \mathcal{T}_\psi^{-1}[\Psi]}{\partial y^2} \right] + k^2 \Psi_n(x) &= 0 \\ n &= 0, 1, 2, \dots \end{aligned} \quad (7)$$

Once these equations have been solved for Ψ_n , the inverse transform eqn (6) is used to find the solution, $\phi(x, y)$.

2.1 Angular spectrum (Fourier–Galerkin) modelling

Here, we will use the Fourier transform for a domain of width $2b$, so that $\psi_n = \cos[\lambda_n(y+b)]$, with $\Psi_n = f_n$, $w = 1$, and $\lambda_n = \frac{1}{2}n\pi/b$. This gives

$$\begin{aligned} f_n(x) &= \mathcal{F}_F[\phi(x, y)] \\ &= \frac{1}{2b} \int_{-b}^b \phi(x, y) \cos[\lambda_n(y+b)] dy \\ n &= 0, 1, 2, \dots \end{aligned} \quad (8)$$

$$\begin{aligned} \phi(x, y) &= \mathcal{F}_F^{-1}[f] \\ &= \sum_{n=0}^{\infty} \epsilon_n f_n(x) \cos[\lambda_n(y+b)] \\ &\text{for } -b < y < b \end{aligned} \quad (9)$$

where $\epsilon_0 = 1$ and $\epsilon_n = 2$ for $n \geq 1$. The $f_n(x)$ are the Fourier modal amplitudes. Since

$$\mathcal{F}_F \left[\frac{\partial^2 \phi}{\partial y^2} \right] = -\lambda_n^2 f_n$$

the governing equations for the Fourier modes simplify. Thus, transforming the Helmholtz eqn (1) gives

$$\frac{d^2 f_n(x)}{dx^2} + (k^2 - \lambda_n^2) f_n(x) = 0 \quad n = 0, 1, 2, \dots \quad (10)$$

This equation shows that each Fourier mode evolves independently of all the others. Solving eqn (10) gives

$$f_n(x) = a_n \exp \left\{ \pm i x \sqrt{k^2 - \lambda_n^2} \right\}, \quad \text{for } n = 0, 1, 2, \dots$$

we take the positive as we are interested in propagation in the $+x$ direction. Only those modes, for which $\lambda_n < k$, represent progressive wave trains; the remainder decay with x . Therefore, the solution procedure is simplified (in the far field) by determining only the progressive modes.

The inverse Fourier transform, eqn (9), provides the final solution,

$$\phi(x, y) = \sum_{n=0}^{\infty} \epsilon_n a_n \exp \left\{ i x \sqrt{k^2 - \lambda_n^2} \right\} \cos[\lambda_n(y+b)]$$

The constants a_n are found from the Fourier transform of the ‘initial condition’, $\phi(0, y) : a_n = \mathcal{F}_F[\phi(0, y)]$. This solution comprises the angular spectrum, which is the superposition of many plane wave trains, each travelling in a direction given by $\tan^{-1}(\lambda_n/\sqrt{k^2 - \lambda_n^2})$. It can also be viewed as the superposition of the fundamental modes of the Laplace equation. This is the *angular spectrum model* for a channel.

The angular spectrum model is indistinguishable in Cartesian coordinates from the separation of variables solution, or an eigenfunction expansion method, since the Fourier series are in fact the eigenfunctions in the lateral direction. Dalrymple²³ used these series

expansions for ϕ to examine waves past channel transitions, and Dalrymple and Martin²⁴ examined waves through a line of offshore breakwaters.

2.2 Chebyshev-tau method

This method begins with

$$\psi_n(y) = T_n(Y) \quad \text{where } Y = y/b \quad (11)$$

and T_n is a Chebyshev polynomial. The Chebyshev transform and its inverse are

$$\begin{aligned} c_n(x) &= \mathcal{T}_C[\phi(x, y)] = \frac{\epsilon_n}{\pi} \int_{-1}^1 \frac{\phi(x, bY) T_n(Y)}{\sqrt{1-Y^2}} dY \\ n &= 0, 1, 2, \dots \end{aligned} \quad (12)$$

$$\begin{aligned} \phi(x, y) &= \mathcal{T}_C^{-1}[c(x)] = \sum_{n=0}^{\infty} c_n(x) T_n(Y) \\ &\text{for } -1 < Y < 1 \end{aligned} \quad (13)$$

For the Chebyshev polynomials, the second derivative does not behave as conveniently as in the Fourier transform. However it can be rewritten in a form which is computationally more convenient (and accurate) for large values of n (see Canuto *et al.*²⁵, p. 69):

$$\frac{\partial^2 \phi}{\partial y^2} = \sum_{n=0}^{\infty} c_n(x) \frac{d^2 T_n(Y)}{dY^2} = \frac{1}{b^2} \sum_{n=0}^{\infty} c_n^{(2)} T_n(Y) \quad (14)$$

where

$$c_n^{(2)} = 2\epsilon_n \sum_{l=1}^{\infty} l(n+l)(n+2l) c_{n+2l}(x) \quad (15)$$

The transformed equation is now

$$\frac{d^2 c_n}{dx^2} + k^2 c_n(x) + \frac{1}{b^2} c_n^{(2)} = 0 \quad n = 0, 1, 2, \dots \quad (16)$$

which is a coupled (through the second derivative) system of equations for the modal amplitudes.

Note that $\psi_n(y)$, defined by eqn (11), does not satisfy the no-flow conditions on the walls; in fact,

$$\psi_n'(-b) = T_n'(-1) = n^2(-1)^{n+1}$$

and

$$\psi_n'(b) = T_n'(1) = n^2$$

In order to enforce the boundary conditions, the Chebyshev-tau method is used,²⁵ which is discussed in Section 4.3.

The Chebyshev-tau method does not offer any advantages for the Helmholtz equation in Cartesian coordinates since *all* modes are progressive, implying that, numerically, many terms must be retained in eqn (13). However, the situation may be different for other coordinate systems or for other equations. Before investigating these possibilities, we introduce the forward-propagation models.

2.3 Forward-propagation models

The governing eqn (7) is a second-order differential equation that requires two boundary conditions. The initial conditions for the amplitudes are readily found by transforming the initial condition, while the other boundary condition, for large x , say, is often unknown *a priori*. Dalrymple and Kirby,⁶ using Fourier transforms, surmounted this problem by splitting the Fourier amplitude $f_n(x)$ into forward-propagating and backward-propagating terms: $f_n = f_n^+ + f_n^-$; these are associated with the positive and the negative signs in the exponent of eqn (4). This leads to first-order differential equations in the split variables, which are also faster to solve numerically than the original second-order equation.

Assume that

$$\begin{aligned}\frac{df_n^+}{dn} &= i\sqrt{k^2 - \lambda^2} f_n^+ + F_n(x) \\ \frac{df_n^-}{dx} &= i\sqrt{k^2 - \lambda^2} f_n^- - F_n(x)\end{aligned}$$

where the function F_n is unknown *a priori*. Substituting into eqn (10) gives $F_n(x) = 0$, so that the second-order equation is split exactly and the forward-propagating mode is correctly given by

$$\frac{df_n^+}{dx} = i\sqrt{k^2 - \lambda^2} f_n^+$$

The solution to this first-order equation depends on the initial condition only (meaning the unknown down-wave boundary condition can be neglected). Moreover, it is exactly the same as that given by separation of variables applied to the Helmholtz equation, showing again that the splitting procedure is exact for this equation.

For the Chebyshev-tau method, the splitting in the transform domain follows the same procedure as before, except that the assumed splitting is different because of the nature of the second derivative in y :

$$\begin{aligned}\frac{dc_n^+}{dx} &= ikc_n^+ + F_n(x) \\ \frac{dc_n^-}{dx} &= -ikc_n^- - F_n(x)\end{aligned}$$

Substituting into eqn (16), the forward-propagating equation is found to be

$$\frac{dc_n^+(x)}{dx} = ikc_n^+(x) + \frac{i}{2kb^2} c_n^{(2)} = 0$$

where only the c_n^+ are used to calculate $c_n^{(2)}$. If we used the first form of the second derivative in eqn (14), this equation would be

$$\frac{dc_n^+(x)}{dx} = ikc_n^+(x) + \frac{i}{2k} \mathcal{T}_C \left[\frac{\partial^2 \mathcal{T}_C^{-1}[c]}{\partial y^2} \right] = 0$$

The inverse transform of this equation is

$$\frac{\partial \phi}{\partial x} = ik\phi + \frac{i}{2k} \frac{\partial^2 \phi}{\partial y^2} = 0$$

which is the small-angle parabolic representation of the Helmholtz equation. Small-angle parabolic models are known to be inaccurate for waves that propagate at large angles to the x -axis. This appears to be a serious consequence of splitting the Chebyshev equation, potentially limiting its effectiveness in forward-propagating models. This same result applies to the variable-depth (mild-slope) equation.

3 THEORY: CONFORMAL MAPPING

In the physical domain, the velocity potential, $\phi(x, y)$, is found by solving the Helmholtz equation in the given complicated geometry. Alternatively, we can map the problem into a conformal domain, which is identified with the independent variables, $u(x, y)$ and $v(x, y)$. The dependent variable becomes $\phi(u, v)$. The mapping procedure is described in the Appendix.^{22,26} For all cases, the channel sidewalls will be mapped into $v = \pm v_b$.

The resulting governing equation in the conformal domain is much the same as that in Cartesian coordinates,

$$\frac{\partial^2 \phi}{\partial u^2} + \frac{\partial^2 \phi}{\partial v^2} + k^2 J \phi = 0 \quad (17)$$

with the exception of the presence of J , which is the Jacobian of the transformation, defined by

$$J(u, v) = \frac{\partial x}{\partial u} \frac{\partial y}{\partial v} - \frac{\partial x}{\partial v} \frac{\partial y}{\partial u} \quad (18)$$

This form of the Helmholtz equation serves as our starting point for developing the various numerical models in the conformal domain.

Note that we can only obtain separated solutions of eqn (17) if $k^2 J$ is of the form

$$k^2 J(u, v) = \mathcal{J}_1(u) + \mathcal{J}_2(v)$$

Then, with $\phi(u, v) = U(u)V(v)$, we obtain the following equations for U and V :

$$U'' + (\mathcal{J}_1 - \lambda^2)U = 0 \quad (19)$$

$$V'' + (\mathcal{J}_2 + \lambda^2)V = 0 \quad (20)$$

In particular, if $\mathcal{J}_2 \equiv 0$, the lateral eigenmodes for the channel are

$$V_n(v) = \cos[\lambda_n(v + v_b)] \quad \text{with} \quad \lambda_n = \frac{1}{2} n\pi / v_b \quad (21)$$

just as for the Cartesian case. Alternatively, if $\mathcal{J}_1 \equiv 0$, then we obtain $U(u) = e^{i\lambda u}$ as a propagating mode; here,

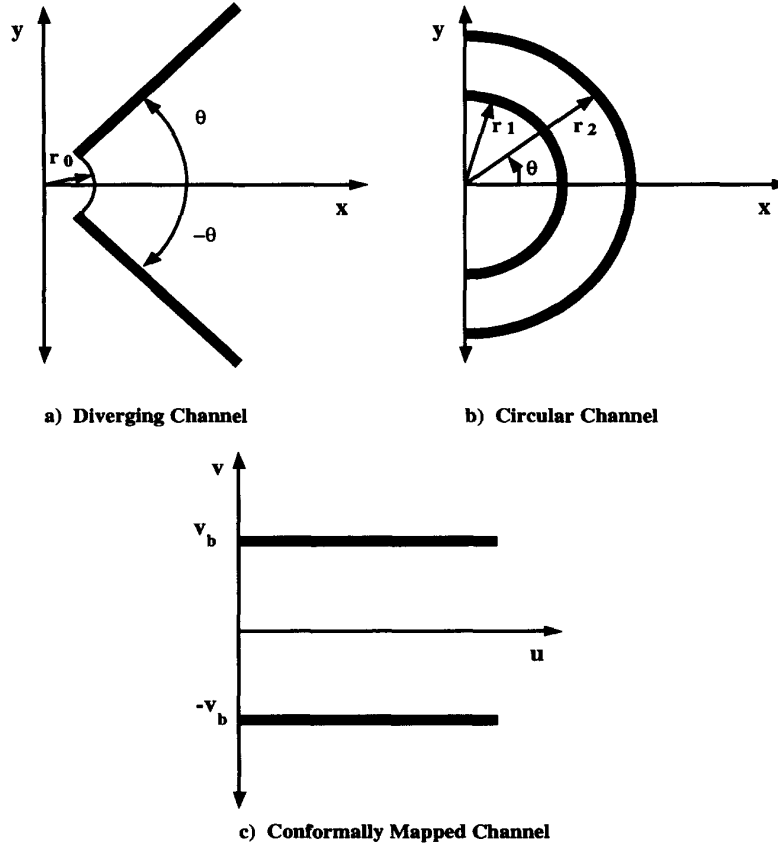


Fig. 1. Schematic diagram of the two examples (top row, (a), (b)) and the conformed channel (c).

we have replaced λ^2 by $-\lambda^2$, giving

$$V'' + (\mathcal{J}_2 - \lambda^2)V = 0$$

as the equation for the lateral modes.

3.1 Examples

A logarithmic conformal map will be used here to illustrate the various spectral approaches to wave modelling. This mapping converts radial lines and circles about the origin in the physical domain into orthogonal straight lines in the mapped domain. Here we provide analytical solutions to two problems to be used as a basis of comparison to the numerical models to be developed in the next section.

3.1.1 The diverging channel

The first example is a constant depth, radially diverging channel with straight vertical impermeable sidewalls. The mapping is $w = \ln(z/r_0)$, where $w = u + iv$, $z = x + iy$ and r_0 is the distance from the origin to the mouth of the channel. The mapping can be rewritten as $u = \ln(r/r_0)$ and $v = \theta$, which, with the exception of the presence of the logarithm, looks like a polar-coordinate transformation. The channel sidewalls lie on $v = \pm v_b = \pm \theta_\ell$. In terms of x and y , the inverse mapping gives $z = r_0 e^w$, or, $x = r_0 e^u \cos v$ and

$y = r_0 e^u \sin v$. In the z -plane, the waves are supposed to propagate in the positive x -direction, while in the mapped domain, the waves will travel primarily in the positive u -direction. See Fig. 1(a).

The Jacobian of the transformation is $J = r_0^2 e^{2u}$, which is a function of u only. Thus, $\mathcal{J}_2 \equiv 0$, whence $V(v) = \cos[\lambda(v + v_b)]$ and

$$U'' + [(kr_0 e^u)^2 - \lambda^2]U = 0$$

which has general solution

$$U(u) = AJ_\lambda(kr_0 e^u) + BY_\lambda(kr_0 e^u)$$

where J_λ and Y_λ are Bessel functions. For rigid walls at $v = \theta = \pm \theta_\ell$ (so that $v_b = \theta_\ell$), and for waves propagating in the direction of u increasing, the solution is readily obtained

$$\phi(r, \theta) = \sum_{n=0}^{\infty} a_n H_{\beta_n}^{(1)}(kr) \cos \beta_n(\theta + \theta_\ell) \quad (22)$$

where $H_\lambda^{(1)} = J_\lambda + iY_\lambda$ and $\lambda = \beta_n$, with $\beta_n = \frac{1}{2}n\pi/\theta_\ell$.

Given the potential at $r = r_0$ as $G(\theta)$, the modal amplitudes are

$$a_m = \frac{\epsilon_m}{2\theta_\ell H_{\beta_m}^{(1)}(kr_0)} \int_{-\theta_\ell}^{\theta_\ell} G(\theta) \cos \beta_m(\theta + \theta_\ell) d\theta \quad \text{for } m = 0, 1, 2, \dots \quad (23)$$

For the case of a planar wave train entering into a diverging channel centred about $\theta = 0$, we taken $G(\theta) = \exp(ikr_0 \cos \theta)$, corresponding to normal incidence.

We note that eqn (22) is the exact linear solution; it can also be obtained by separation of variables of eqn (1) in plane polar coordinates.²²

3.1.2 The circular channel

The second example is a constant depth channel with vertical sidewalls laid out in a circular planform. Let r_1 and r_2 be the inner and outer radius of the channel, respectively. The waves are supposed to propagate primarily counter-clockwise in the axial (θ) direction, from the mouth of the channel located at $\theta = -\pi/2$. In the mapped domain, the channel is straight, with the waves again propagating in the positive u -direction, as shown in Fig. 1(b). Here the conformal map is somewhat different (to keep the same u principal propagation direction): $w = \pi/2 - i \ln(z/r_m)$, where $r_m = \sqrt{r_1 r_2}$. This corresponds to $u = \pi/2 + \theta$ and $v = \ln(r_m/r)$. The outer sidewall of the channel is mapped to $v = -v_b = \ln(r_m/r_2) = -\frac{1}{2} \ln(r_2/r_1)$, while the inner wall is mapped to $v = v_b$. In terms of z , we have $z = r_m e^{i(w-\pi/2)}$, which leads to $x = r_m e^{-v} \sin u$ and $y = -r_m e^{-v} \cos u$.

The Jacobian of this transformation is $J = r_m^2 e^{-2v}$, which is a function of v only. Thus, $\mathcal{J}_1 \equiv 0$, whence

$$U(u) = e^{i\lambda u} \quad (24)$$

for propagation in the direction of u increasing. $V(v)$ satisfies

$$V'' + [(kr_m e^{-v})^2 - \lambda^2] V = 0 \quad (25)$$

which has general solution

$$V(v) = AJ_\lambda(kr_m e^{-v}) + BY_\lambda(kr_m e^{-v})$$

At the outer wall $r = r_2$, we have $v = \frac{1}{2} \ln(r_1/r_2) = -v_b$ and $V'(-v_b) = 0$; therefore

$$V(v) = Y'_\lambda(kr_2)J_\lambda(kr_m e^{-v}) - J'_\lambda(kr_2)Y_\lambda(kr_m e^{-v})$$

At the inner wall $r = r_1 < r_2$, we have $v = v_b$ and $V'(v_b) = 0$, giving

$$Y'_\lambda(kr_1)J'_\lambda(kr_2) - J'_\lambda(kr_1)Y'_\lambda(kr_2) = 0 \quad (26)$$

This is an equation for λ . It is known that eqn (26) has discrete roots; call them $\lambda = \alpha_n$, with $n = 0, 1, 2, \dots$. There are only a finite number of real roots ($0 < \alpha_n < kr_2$); these give the propagating modes. Equation (26) also has an infinite number of purely imaginary solutions; those with positive imaginary parts give the evanescent modes. These solutions have been discussed by Buchholz²⁷ in the context of curved electromagnetic wave guides, and by Rostafinski²⁸ in the context of acoustics.

Ordering the real eigenvalues from the largest to the smallest, we find that the first eigenvalue corresponds to the zeroth mode, which has no zero crossing in the transverse (radial) direction. Therefore the mode looks like a propagating wave train, but confined to the outer wall; it is the annular equivalent of the 'whispering gallery mode' as it is large on the outer radius and decays rapidly and monotonically in the (negative) r -direction. The next eigenvalue corresponds to the first mode, with one zero crossing, and so on.

The problem of solving eqn (25), together with $V'(\pm v_b) = 0$, is a Sturm-Liouville problem. Let $V_n(v)$

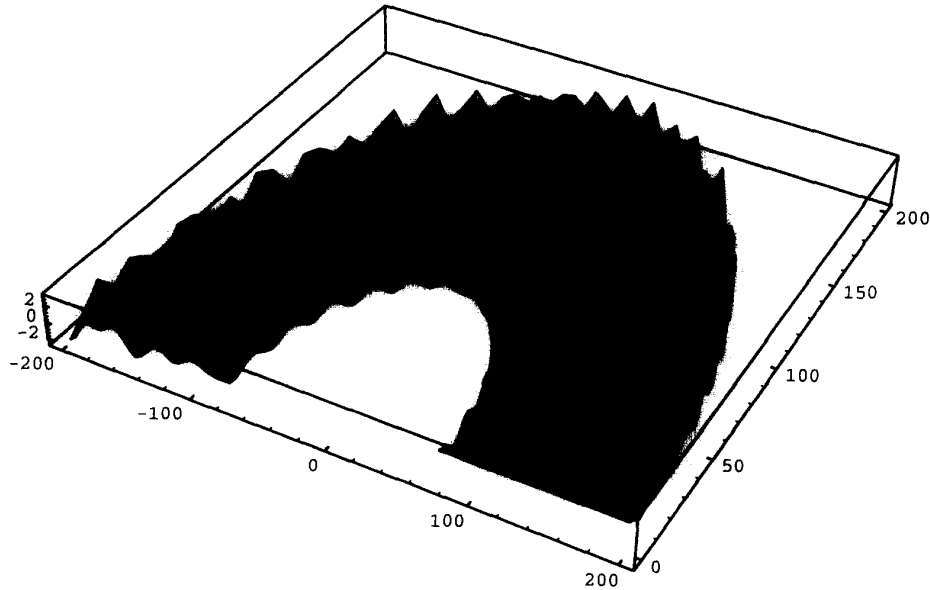


Fig. 2. Exact solution for waves in a wide circular channel.

be a solution corresponding to $\lambda = \alpha_n$,

$$V_n(v) = A_n \{ Y'_{\alpha_n}(kr_2) J_{\alpha_n}(kr_m e^{-v}) - J'_{\alpha_n}(kr_2) Y_{\alpha_n}(kr_m e^{-v}) \} \quad (27)$$

(recall that $r = r_m e^{-v}$). These eigenfunctions are orthogonal,

$$\int_{-v_b}^{v_b} V_m(v) V_n(v) dv = 0 \quad \text{for } \alpha_m \neq \alpha_n$$

and the constant A_n can be chosen so that

$$\int_{-v_b}^{v_b} V_n^2(v) dv = 1$$

They are also complete, so that we have

$$\phi(u, v) = \sum_{n=0}^{\infty} a_n e^{i\alpha_n u} V_n(v) \quad (28)$$

At the beginning of the channel, $u = 0$ ($\theta = -\pi/2$), we have $\phi(0, v) = G(v)$, say, whence

$$a_n = \int_{-v_b}^{v_b} G(v) V_n(v) dv \quad (29)$$

Again, this solution is exact; it can also be obtained by separation of variables of eqn (1) in plane polar coordinates.²²

In Fig. 2, the exact linear solution for the wave field is shown for waves incident into a 180° turn. As the waves enter the channel, they begin to reflect from the outer wall and diffract in the vicinity of the inner wall.

4 NUMERICAL MODELLING IN THE CONFORMAL DOMAIN

4.1 Fourier–Galerkin approach

Following Dalrymple *et al.*,⁷ where a Helmholtz equation with variable coefficients (arising due to bottom variations) was treated, we define a lateral average of the variable coefficient in the conformal Helmholtz eqn (17) by

$$\overline{k^2 J}(u) = \frac{1}{2v_b} \int_{-v_b}^{v_b} k^2 J(u, v) dv \quad (30)$$

Substituting this into the governing eqn (17) gives

$$\frac{\partial^2 \phi}{\partial u^2} + \frac{\partial^2 \phi}{\partial v^2} + \overline{k^2 J}(1 - \nu) \phi = 0 \quad (31)$$

where

$$\nu(u, v) = 1 - k^2 J / \overline{k^2 J} \quad (32)$$

incorporates the lateral variability of the original coefficient, $k^2 J$.

We suppose, as before, that the boundaries at $v = \pm v_b$ are impermeable (so that $\partial \phi / \partial v = 0$). Then, the

appropriate Fourier-transform pair is the following (cf. eqns (8) and (9)):

$$\begin{aligned} f_n(u) &= \mathcal{F}_F[\phi(u, v)] \\ &= \frac{1}{2v_b} \int_{-v_b}^{v_b} \phi(u, v) \cos[\lambda_n(v + v_b)] dv \\ n &= 0, 1, 2, \dots \end{aligned} \quad (33)$$

$$\begin{aligned} \phi(u, v) &= \mathcal{F}_F^{-1}[f(u)] \\ &= \sum_{n=0}^{\infty} \epsilon_n f_n(u) \cos[\lambda_n(v + v_b)] \\ &\quad \text{for } -v_b < v < v_b \end{aligned} \quad (34)$$

Transforming eqn (31) yields

$$\begin{aligned} \frac{d^2 f_n}{du^2} + \gamma_n^2 f_n - \overline{k^2 J} \mathcal{F}_F[\nu \mathcal{F}_F^{-1}[f]] &= 0 \\ n &= 0, 1, 2, \dots \end{aligned} \quad (35)$$

where

$$\gamma_n^2(u) = \overline{k^2 J} - \lambda_n^2 \quad \text{and} \quad \lambda_n = \frac{1}{2} n \pi / v_b$$

The set of eqns (35) is exactly equivalent to eqn (31), provided the series (34) converges. The last term in eqn (35), which adds complexity to the solution, results from the Fourier transform of a product of two functions of v .

To obtain a forward-propagation model, we separate f_n into forward- and backward-propagating wave modes as before and keep only the forward-propagating modes to yield

$$\begin{aligned} \frac{df_n^+(u)}{du} &= \left(i\gamma_n - \frac{1}{2\gamma_n} \frac{d\gamma_n}{du} \right) f_n^+ \\ &\quad - \frac{ik^2 J}{2\gamma_n} \mathcal{F}_F[\nu \mathcal{F}_F^{-1}[f^+]] \quad n = 0, 1, 2, \dots \end{aligned} \quad (36)$$

This final set of equations governs the propagating Fourier modes in a conformal domain. The equations are approximate due to the neglect of the backward-propagating modes that occur in the last term; this term couples all the modes and can result in the growth of modes that may have been originally zero at $u = 0$.

The initial conditions on $f_n(u)$ are provided by a Fourier transform of the given initial condition, $\phi(0, v) = G(v)$, say, giving

$$f_n(0) = \frac{1}{2v_b} \int_{-v_b}^{v_b} G(v) \cos[\lambda_n(v + v_b)] dv \quad n = 0, 1, 2, \dots$$

Suppose that $\nu \equiv 0$, that is, $k^2 J$ is independent of v , the lateral coordinate. Then, as we have seen in Section 3 (the case $\mathcal{J}_2 \equiv 0$), eqn (31) is separable: the lateral eigenfunctions of the problem, $V_n(v)$, satisfying the sidewall conditions, $V'(v) = 0$ at $v = \pm v_b$, are given by eqn (21). In other words, for this particular case, the actual lateral eigenfunctions are the same cosines as

used in the Fourier-transform pair, eqns (33) and (34). It follows that the convergence of the method is guaranteed. However, for other problems, in which $\nu \neq 0$, the solution may not be separable and, if it is, the actual lateral eigenfunctions will differ from eqn (21); consequently, we expect some errors in the method.

4.2 Angular spectrum approach

In Cartesian coordinates, the angular spectrum method and the Fourier–Galerkin approach are the same. However, in other coordinate systems, this may not be true. The angular spectrum method is then interpreted as an eigenfunction expansion method, with the eigenfunctions determined by the lateral Sturm–Liouville problem, eqn (20). The advantage of the angular spectrum method is that the lateral eigenfunctions are the exact solutions for the problem. The disadvantage in transformed coordinates is that it is unlikely that there are fast algorithms (equivalent to the FFT) for obtaining eigenfunction expansions.

4.3 Chebyshev-tau approach

It is known that the Chebyshev polynomials, $T_n(\zeta)$, $n = 0, 1, 2, \dots$, are a complete orthogonal basis over the range $-1 \leq \zeta \leq 1$. Their use requires a preliminary scaling of the problem,

$$\zeta = v/v_b$$

so that the lateral boundaries are located at $\zeta = \pm 1$. The appropriate Chebyshev-transform pair is (cf. eqns (12) and (13)):

$$\begin{aligned} c_n(u) &= \mathcal{T}_C[\phi(u, v)] \\ &= \frac{\epsilon_n}{\pi} \int_{-1}^1 \frac{\phi(u, v_b \zeta) T_n(\zeta)}{\sqrt{1 - \zeta^2}} d\zeta \quad n = 0, 1, 2, \dots \end{aligned} \quad (37)$$

$$\begin{aligned} \phi(u, v) &= \mathcal{T}_C^{-1}[c(u)] \\ &= \sum_{n=0}^{\infty} c_n(u) T_n(\zeta) \quad \text{for } -1 < \zeta < 1 \end{aligned} \quad (38)$$

As the Chebyshev polynomials do not satisfy the lateral boundary conditions, a straightforward Galerkin technique is precluded. The tau method forces the Chebyshev sum to satisfy these conditions, and will be discussed below.

Introducing $k^2 J$ and ν , defined by eqns (30) and (32), respectively, we find that the Chebyshev transform of eqn (31) is

$$\frac{d^2 c_n(u)}{du^2} + k^2 J c_n(u) + \frac{1}{v_b^2} c_n^{(2)} - k^2 J \mathcal{T}_C[\nu \mathcal{T}_C^{-1}[c]] = 0$$

The splitting in the transform domain follows as before:

$$\begin{aligned} \frac{dc_n^+}{du} &= \left(i\gamma_0 - \frac{1}{2\gamma_0} \frac{d\gamma_0}{du} \right) c_n^+(u) \\ &+ \frac{i}{2\gamma_0} \left(\frac{1}{v_b^2} c_n^{(2)} - k^2 J \mathcal{T}_C[\nu \mathcal{T}_C^{-1}[c^+]] \right) = 0 \end{aligned} \quad (39)$$

This equation is less accurate than that obtained from the Fourier–Galerkin splitting. Note that the first term on the right-hand side of eqn (39) is proportional to γ_0 instead of γ_n , as the second derivative of T_n does not yield a term proportional to c_n directly as occurs with the trigonometric functions in the Fourier–Galerkin approach.

At $|\zeta| = 1$, $\partial\phi/\partial\zeta = 0$ so as to satisfy the no-flow channel boundary conditions. Since the Chebyshev polynomials do not satisfy these lateral boundary conditions individually (as the Fourier modes do), we use the Chebyshev-tau method to enforce them.²⁵ First, truncate the series in eqn (38) to give

$$\phi(u, v) = \sum_{n=0}^N c_n(u) T_n(\zeta)$$

With this approximation, the no-flow conditions at $\zeta = \pm 1$ yield

$$\sum_{n=1}^N n^2 c_n(u) = 0 \quad \text{and} \quad \sum_{n=1}^N (-1)^n n^2 c_n(u) = 0$$

These two equations are used to specify $c_{N-1}(u)$ and $c_N(u)$ in terms of the remaining coefficients, which are themselves determined by integrating eqn (39) for $0 \leq n \leq N-2$; we used a fourth-order Runge–Kutta scheme. The step size du depended on the number of modes computed, with a smaller step size required for a solution with more modes.

The Chebyshev transforms are carried out numerically using Gauss quadrature:

$$\int_{-1}^1 \frac{g(\zeta)}{\sqrt{1 - \zeta^2}} d\zeta \simeq \sum_{i=1}^M w_i g(\zeta_i)$$

The Gauss points ζ_i are the zeros of $T_M(\zeta)$, namely

$$\zeta_i = \cos\left(\frac{(2i-1)\pi}{2M}\right) \quad i = 1, 2, \dots, M$$

and $w_i = \pi/M$ for all i (Abramowitz & Stegun,²⁹ Chap. 25). For all calculations in this paper, $M = 41$, so that the quadrature error is negligible.

5 DIVERGING CHANNEL

For the case of the diverging channel, the angular spectrum, Fourier–Galerkin and Chebyshev-tau

methods will be compared to the exact solution, which is given by eqns (22) and (23).

5.1 Fourier–Galerkin and angular spectrum models

With the mapping that we have used, $w = \ln(z/r_0)$, the product $k^2 J$ is independent of v and so $\nu \equiv 0$; therefore, the last term in the equation for the Fourier modes, eqn (36), vanishes. The remaining terms (with the superscript + dropped for convenience) can be written as

$$\frac{df_n(u)}{du} = \left(i\gamma_n - \frac{1}{2\gamma_n^2} k^2 r_0^2 e^{2u} \right) f_n(u) \quad n = 0, 1, 2, \dots \quad (40)$$

where

$$\gamma_n = \sqrt{k^2 r_0^2 e^{2u} - \beta_n^2}$$

since $\lambda_n = \beta_n = \frac{1}{2} n\pi/\theta_L$.

For this case, modes not present in the initial conditions cannot arise subsequently. Further, the Fourier cosine series in the lateral direction used in the Fourier transforms eqns (33) and (34) are exact solutions of the associated Sturm–Liouville problem in the v -direction, guaranteeing convergence and also showing the equivalence of the Fourier–Galerkin and the angular spectrum (eigenfunction expansion) approaches for this case.

Equation (40) is a first-order equation for each of the Fourier modes. It can be solved analytically to give

$$f_n(u) = g_n \gamma_n^{-1/2} \exp\{i(\gamma_n - \beta_n \tan^{-1}(\gamma_n/\beta_n))\} \quad n = 0, 1, 2, \dots \quad (41)$$

and then the potential is found from the inverse transform, eqn (34). Note that, for large u and fixed n , we have $\gamma_n \sim k r_0 e^u = kr$ and

$$f_n(u) \sim g_n (kr)^{-1/2} \exp\{i(kr - \beta_n \pi/2)\}$$

which is the far-field approximation to $H_{\beta_n}^{(1)}(kr)$, apart from a constant factor. Therefore, we expect an exact correspondence among the angular spectrum method, the Fourier–Galerkin method, and the exact linear solution for this example.

5.2 Chebyshev-tau method

From eqn (39), the governing equation for each of the Chebyshev modes is

$$\frac{dc_n(u)}{du} = \left(i\gamma_0 - \frac{1}{2} \right) c_n(u) + \frac{i}{2v_b^2 \gamma_0} c_n^{(2)} = 0 \quad n = 0, 1, 2, \dots \quad (42)$$

For the case of normal wave incidence, the solution is symmetric about $\zeta = 0$, and so the coefficients of all the odd Chebyshev polynomials are zero.

5.3 Results

One possible wave motion in the diverging channel is the axisymmetric case of circular waves emanating from $r = 0$, with constant amplitude and phase along any circular arc. The initial condition is taken as $G(\theta) = 1$. The linear wave motion is given analytically in eqn (22) and most conveniently by the leading term, the Hankel function, $H_0^{(1)}(kr)$, where $r = \sqrt{x^2 + y^2}$. All of the numerical methods model this solution correctly in the far field, giving

$$\phi(u, v) = \exp(ik e^u - \frac{1}{2}u)$$

which is the far-field expansion of the Hankel function. In the mapped domain, the wave form is constant along lines of constant u , and no diffraction occurs.

On the other hand, if a plane wave enters the diverging channel, then diffraction occurs as the physical domain becomes wider in the propagation direction. This situation was modelled by Kaku and Kirby³⁰ in a wave tank (see also the description by Kirby *et al.*²²). In a water depth of 0.15 m, vertical plywood breakwaters enclosed a 90° sector, with a mouth of width 1.74 m. A planar wave generator sent waves directly down the centreline. Measurements were made using wavegauges at fixed r locations for several wave cases. Here, we use the most linear set of tests for which the wave period was 0.49 s, and the initial wave amplitude was 0.0085 m. The measurement stations correspond to $r/r_0 = (1.38, 1.87, 2.2)$, where $r_0 = 1.23$ m, taken as the distance from the origin of the polar coordinate system to the breakwaters, and at 10° increments from the centreline.

For the models, the plane wave initial condition of $\phi = \exp(ikr_0 \cos \theta)$ was used. In Fig. 3, the exact water surface elevation is shown for the data of Kaku and Kirby³⁰ in the transformed domain, where there is an apparent focussing of the wave form down the centreline, which is due to the widening of the channel with r in the physical domain. In Fig. 4, the angular spectrum (Fourier–Galerkin) model predictions for water surface elevations are compared to the exact theory and the data of Kaku and Kirby.³⁰ The Fourier–Galerkin model gives, as expected, the same result as the exact solution. In comparing with the parabolic models of Kirby *et al.*,²² the Fourier–Galerkin model is better, as the parabolic models do not replicate the exact theory.

The Fourier–Galerkin model was run with a step size corresponding to $k dr = 0.2136$, where, for this water depth and wave period, the dispersion relationship gives $k = 16.94 \text{ m}^{-1}$. Only the seven progressive modes were used.

For the Chebyshev-tau model, 15 even modes were used ($N = 28$). For this high number of modes, a very small step size in u was required, $du = 0.00178677$; this required about 500 steps to span the measurement

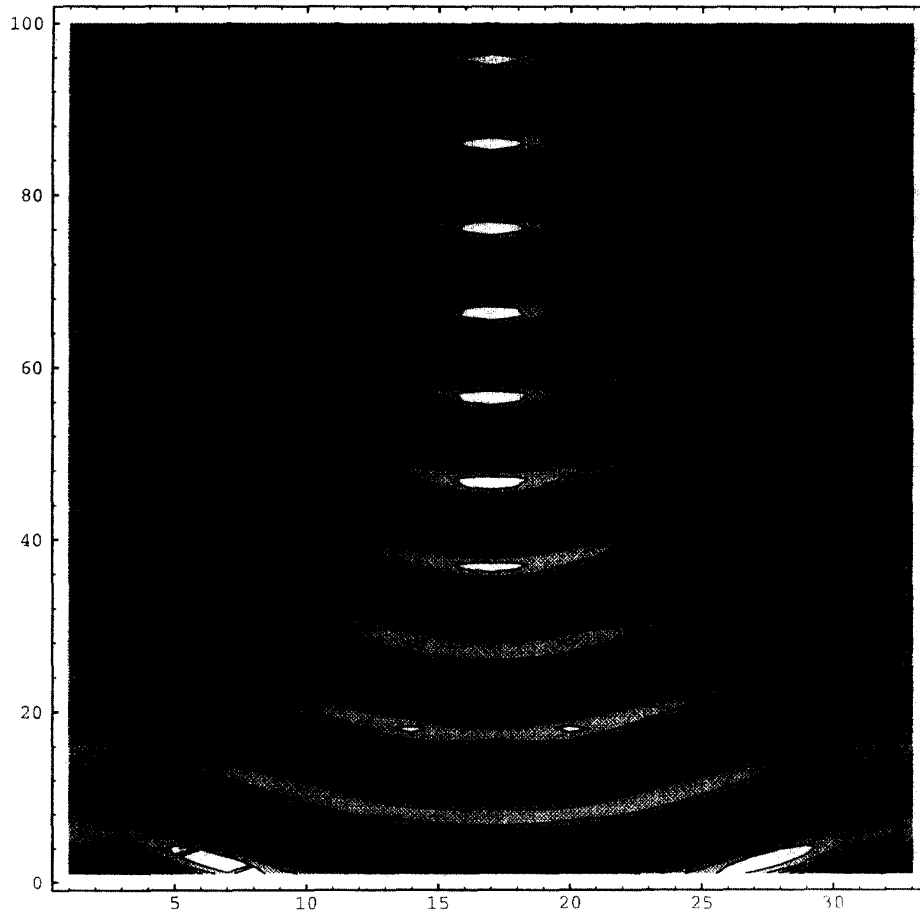


Fig. 3. Instantaneous water surface of diverging channel in mapped domain.

locations — more than required by the Fourier–Galerkin method by almost a factor of three. In Fig. 5, the Chebyshev solution is compared to experimental data³⁰ and to the exact solution. Clearly, there is a discrepancy between the Chebyshev solution and the exact solution, due to the presence of a lateral oscillation in the solution.

6 CIRCULAR CHANNEL

The exact linear solution for this case is given by eqn (28), with eqns (27) and (29). Again, the Fourier–Galerkin and the Chebyshev-tau methods will be compared against this exact solution. In the following examples, the initial condition is a wave train with constant amplitude across the channel, or $G = 1$ in eqn (29).

6.1 Fourier–Galerkin model

As J is not a function of u for this case, the governing

eqn (36) reduces to

$$\frac{df_n(u)}{du} = i\gamma_n f_n - \frac{ik^2 J}{2\gamma_n} \mathcal{F}_F[\nu \mathcal{F}_F^{-1}[f]]$$

$$n = 0, 1, 2, \dots \quad (43)$$

where

$$\overline{k^2 J} = \frac{k^2(r_2^2 - r_1^2)}{2 \ln(r_2/r_1)}$$

and

$$\nu(v) = 1 - \frac{2 \ln(r_2/r_1) r_1 r_2 e^{-2v}}{r_2^2 - r_1^2}$$

since $v_b = \frac{1}{2} \ln(r_2/r_1)$. Now, the Fourier modes, $\{\cos[\lambda_n(v + v_b)]\}$, $n = 0, 1, 2, \dots$, no longer satisfy the exact Sturm–Liouville problem in the lateral direction, which is eqn (25) together with $V'(\pm v_b) = 0$; the Fourier–Galerkin method no longer is the same as the angular spectrum method and the method will have problems with convergence, depending on the size of ν ;

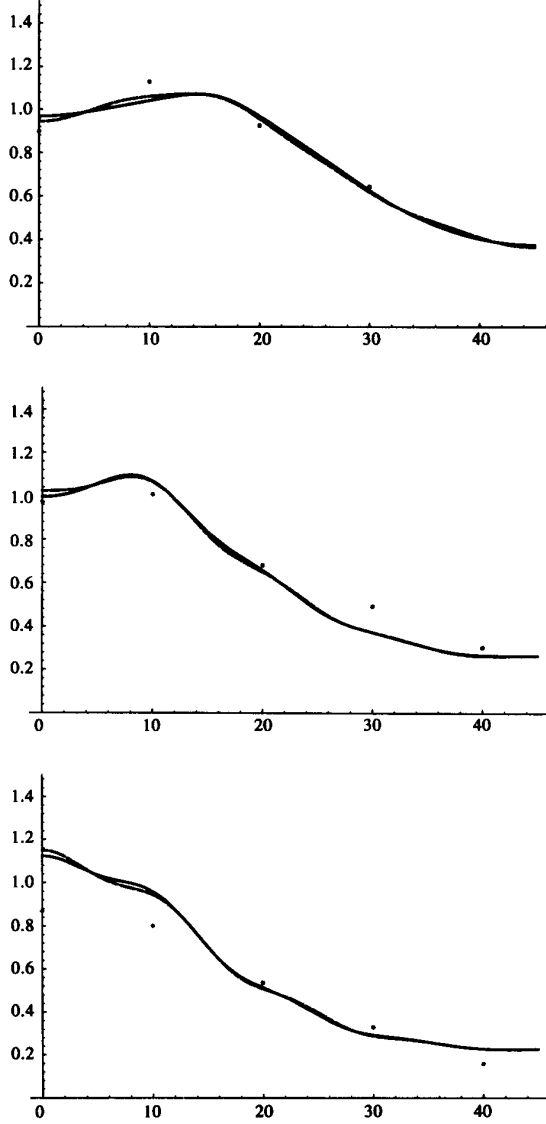


Fig. 4. Comparisons of the angular spectrum model (dashed line), the exact solution (solid line) and the data of Kaku and Kirby³⁰ at $r = 1.38, 1.87, 2.2$ m from top figure to bottom.

we have

$$1 - \frac{2r_2^2 \ln(r_2/r_1)}{r_2^2 - r_1^2} \leq \nu(v) \leq 1 - \frac{2r_1^2 \ln(r_2/r_1)}{r_2^2 - r_1^2} \quad \text{for } r_1 \leq r \leq r_2$$

6.2 Angular spectrum model

The actual lateral eigenfunctions for this problem are given by eqn (27). The propagating modes are given by eqn (24). For the present case of a constant depth channel, the angular spectrum and the exact solution are identical.

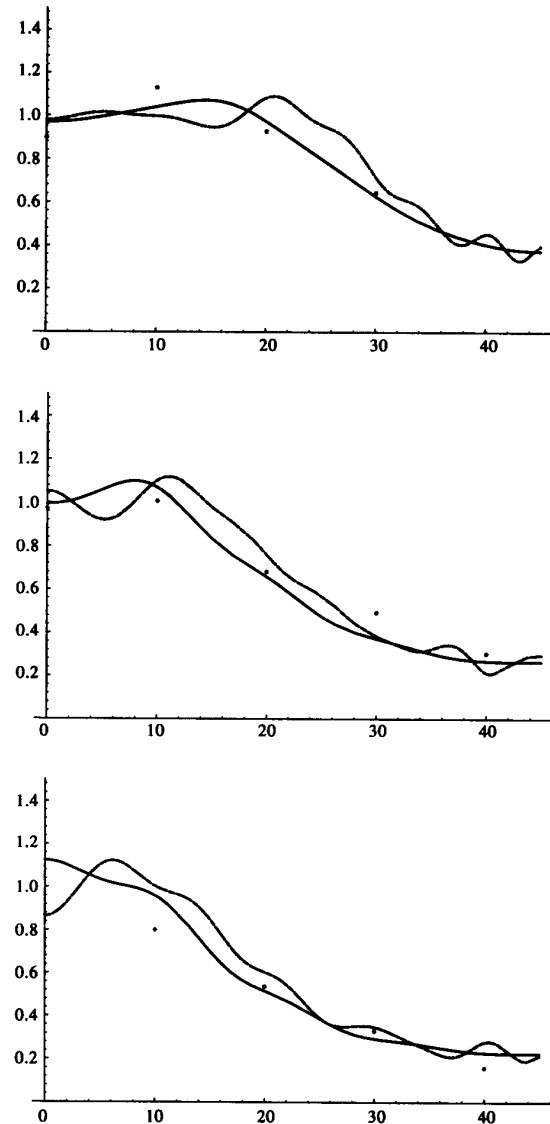


Fig. 5. Comparisons of the Chebyshev model (dashed line), the exact solution (solid line) and the data of Kaku and Kirby³⁰ at $r = 1.38, 1.87, 2.2$ m from top figure to bottom.

6.3 Chebyshev model

The governing equation is obtained from eqn (39):

$$\frac{dc_n(u)}{du} = i\gamma_0 c_n(u) + \frac{i}{2\gamma_0} \left(\frac{1}{v_b^2} c_n^{(2)} - \overline{k^2 J} \mathcal{T}_C[\nu \mathcal{T}_C^{-1}[c]] \right) = 0 \quad (44)$$

with

$$\overline{k^2 J} = \frac{k^2 r_1 r_2 \sinh(2v_b)}{2v_b}$$

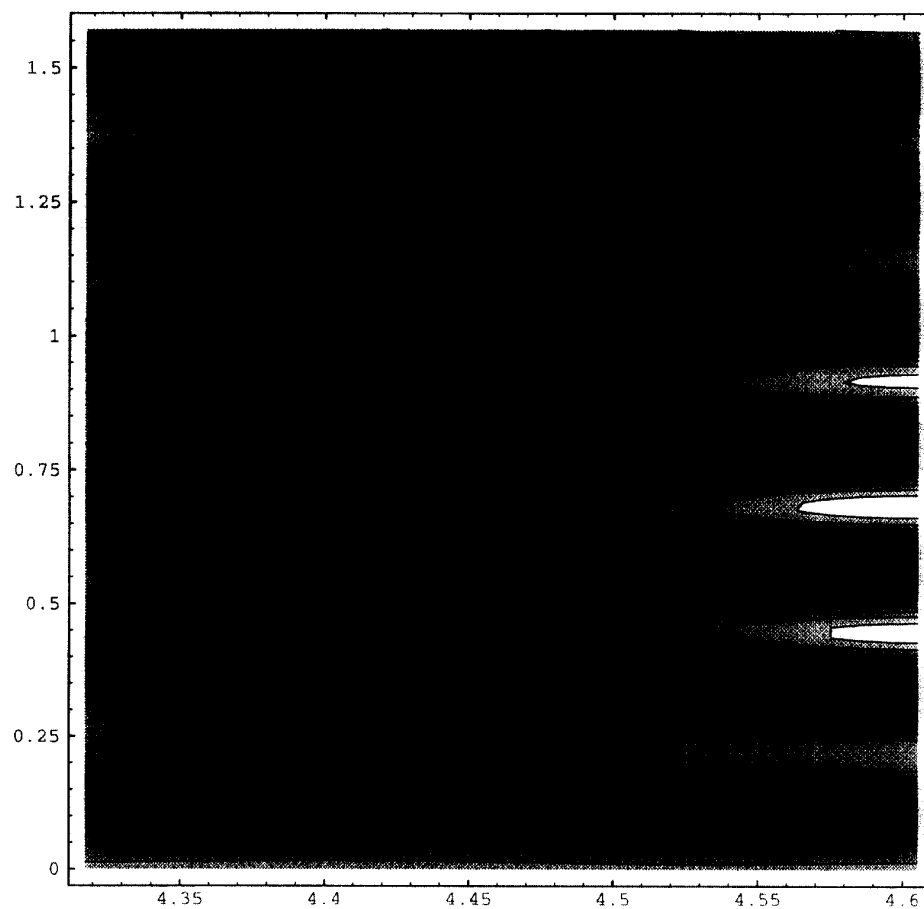


Fig. 6. Exact solution in (u, v) plane for waves in a wider circular channel.

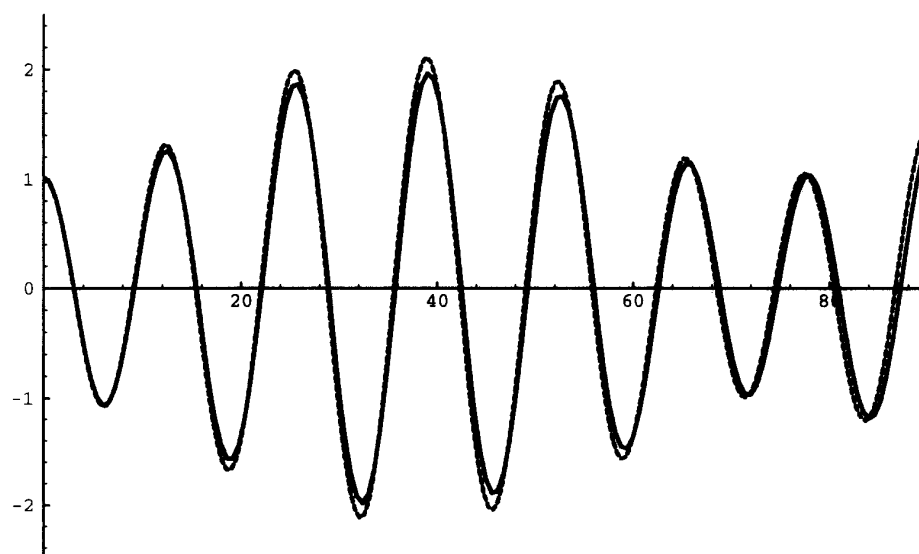


Fig. 7. Comparison of water surface elevation along outer wall between the exact solution and the Fourier-Galerkin model (dashed line) for wider channel.

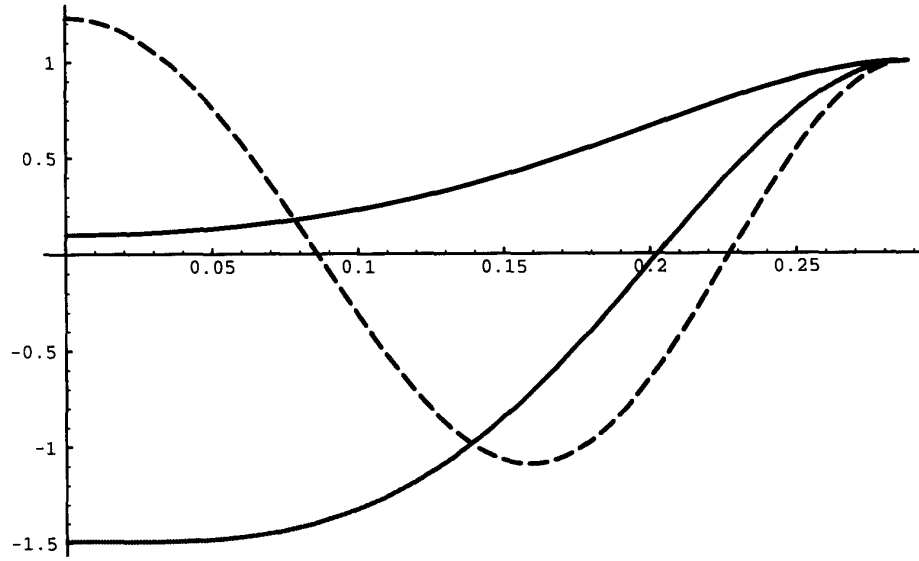


Fig. 8. Three analytical eigenfunctions for the wider channel.

6.4 Results

6.4.1 Narrow and wide channels

A narrow channel is defined as a channel with a width smaller than the wavelength of the incident wave, or $k(r_2 - r_1) < 2\pi$, where the left-hand side is 2π times the number of wavelengths that can fit across the channel. This can be rewritten as $kr_1\delta < 2\pi$, where δ is the dimensionless channel width: $\delta = (r_2 - r_1)/r_1$. In a narrow channel, the waves propagate around the channel with very little change in wave form. For example, given $r_1 = 75$ m, $r_2 = 80$ m, a water depth of 4 m and a wave period of 4 s, $kr_1\delta = 1.5$ and the wave propagates within the channel with little change in form

(the wave amplitude along the outside wall is only 3% greater than elsewhere). The Fourier–Galerkin model and the analytic (exact) model (with only one progressive mode) are indistinguishable for this case.

For a wider channel, obtained by increasing r_2 to 100 m, $kr_1\delta = 7.53$, which corresponds to a channel wider than a wavelength. For this case, the wave field is significantly different, largely due to the much greater distance encompassed by the outer radius than the inner. The ratio of the distances (circumferences) is $r_2/r_1 = \delta + 1$, which is 1.33 in this case; therefore, δ measures the percentage increase in length of the outer circumference over the inner one, or it is a measure of the longer path followed by waves on the outer side of

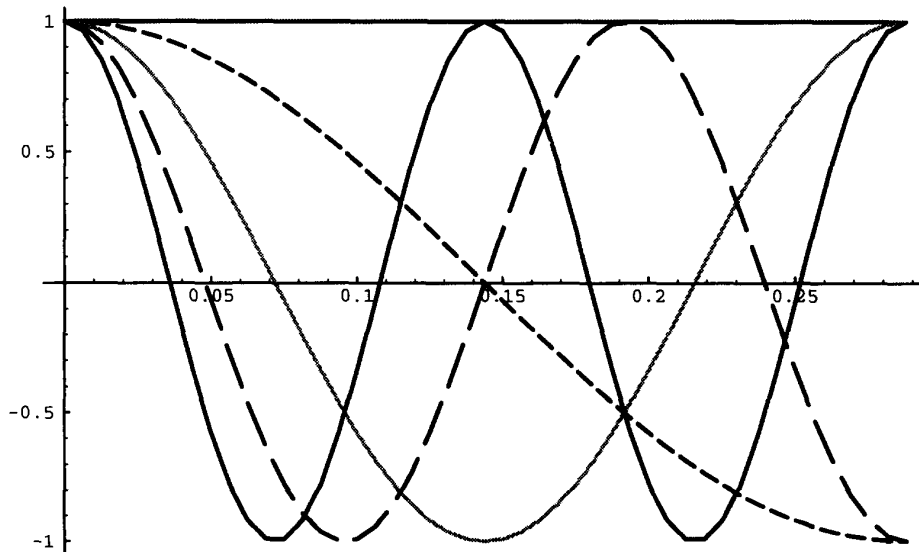


Fig. 9. Eigenfunctions for waves in a wider circular channel in angular spectrum model.

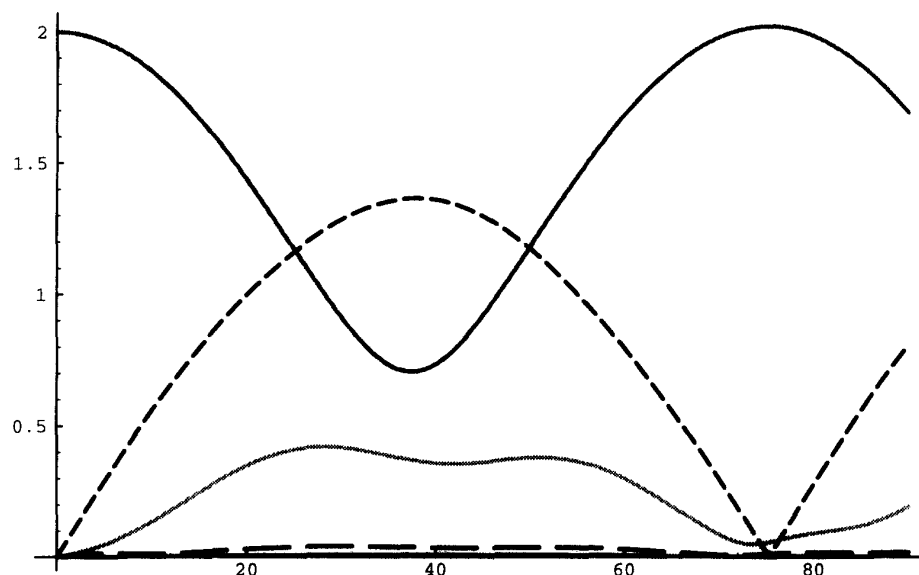


Fig. 10. Variation of the first five Fourier modes in the wider channel as a function of angle.

the channel than the inside. Figure 6 shows an instantaneous snapshot of the free surface (analytical model), which is comprised of three progressive modes. Of particular note is the so-called amphidromic point³¹ in the wave phase that occurs where the 'extra' wave appears along the outer radius (to the right on the figure).

Figure 7 shows the water surface elevation along the outer circumference as predicted by the Fourier–Galerkin model and the analytical model for $0^\circ \leq \theta \leq 90^\circ$. The agreement is quite good, with the Fourier–Galerkin model slightly underpredicting the maxima and propagating slightly faster than the exact solution. For this case, $k^2 J = 689.8$.

In Figure 8, the three lateral eigenfunctions comprising the analytical solution, eqn (28), are shown. In comparison, the Fourier cosines for the Fourier–Galerkin model are shown in Fig. 9. The difference between the general shapes of the eigenfunctions is not large; however, the behaviour of the coefficients multiplying these eigenfunctions is very different. For the analytical model, the a_n values are constant, and the variation of the wave form with θ is due to the superposition of the different modes comprising the solution. For the Fourier–Galerkin model, with its imperfect Fourier series, the Fourier coefficients exchange energy along the channel according to eqn (43), see Fig. 10.

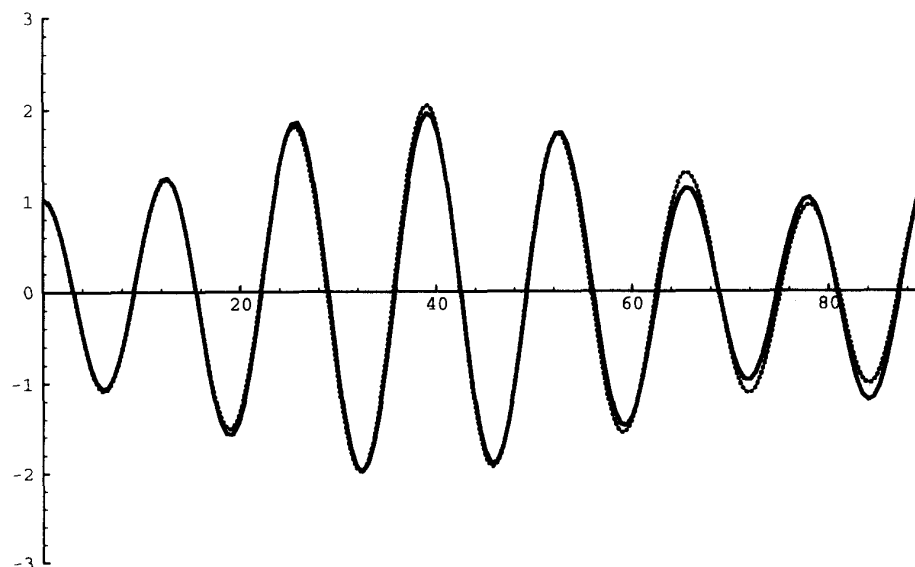


Fig. 11. Comparison of water surface elevation along outer wall between the exact solution and the Chebyshev–tau model (dashed line) for wider channel.

The Chebyshev-tau comparison for the water surface elevation along the outer wall is shown in Fig. 11. Ten Chebyshev polynomials were used for this solution; the use of only eight polynomials gives the same solution.

6.4.2 Very wide channels

Waves in a very wide channel begin to experience diffraction and strong reflection. For this example, $r_2 = 200$ m, so $kr_1\delta = 37.6$, and $\delta = 1.67$. The analytic solution has 12 progressive modes for this case. The waves in the wide (six wave lengths) circular channel initially propagate in a straight line, but as the channel bends, the waves start to diffract around the bend and simultaneously run into the curving channel sidewall to reflect around the bend. Different parts of the wave crest reflect at different times, leading to a complicated sea-state far along the channel. The instantaneous water surface from the exact solution in the physical domain is shown in Fig. 2. The water surface is shown in the conformal domain in Fig. 12.

The Fourier–Galerkin model does not yield a very good solution for this case, due to the large variation in k^2J over the channel width. The Fourier–Galerkin

method assumes that the lateral variation of the solution is expressible in terms of the Fourier series in the v coordinate (which look similar to those in Fig. 9). The actual shapes of the eigenfunctions (obtained from the exact solution) are shown in Fig. 13 and are those used in the angular spectrum model. The very different nature of these eigenfunctions implies that trigonometric bases are not efficient for this case.

The water surface elevations along the outer wall computed by the Fourier–Galerkin model are compared to the exact solution in Fig. 14. Clearly, there is a discrepancy, with the Fourier–Galerkin waves having a faster phase variation than the exact solution. The largest discrepancy occurs at about 38° . (The numerical model was run with grid sizes: $du = 0.452^\circ$, $dv = 0.0377^\circ$.)

Figure 15 shows the results of the Chebyshev-tau model for the wide channel. Here, $N = 20$, $M = 41$ and $du = d\theta = 0.00394$ radians. Clearly, the model has a phase error, which leads to wide discrepancies at 45° . It is likely that this error is largely due to the errors developed in the splitting process and the correspondence to the small-angle parabolic model, which is exacerbated in this case due to the variable nature of

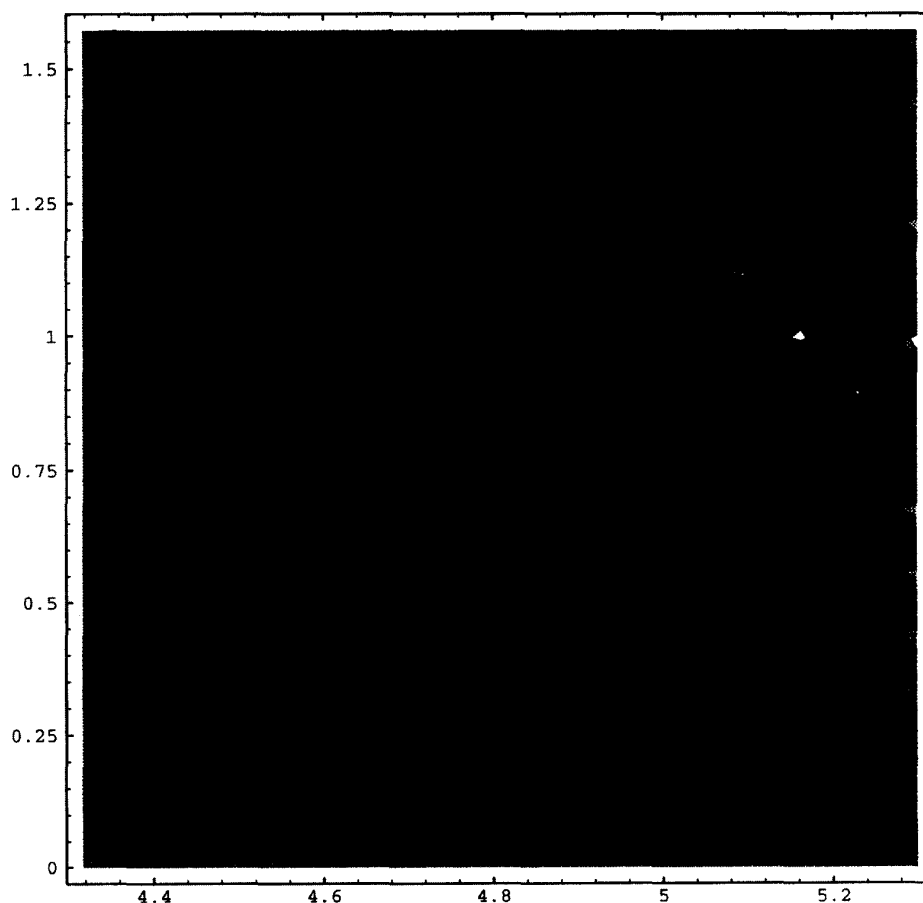


Fig. 12. Exact solution for waves in a wide circular channel in the transform domain.

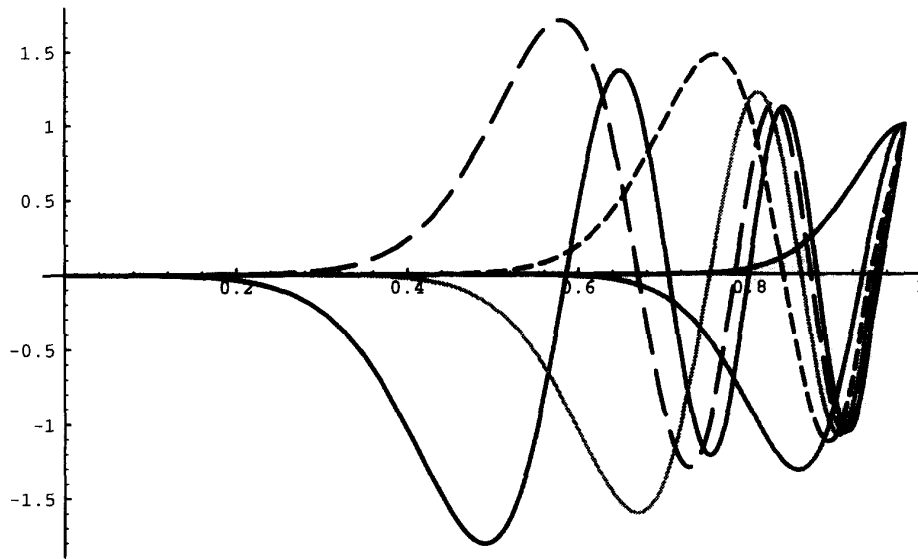


Fig. 13. Eigenfunctions for waves in a wide circular channel.

$k^2 J$. Kirby *et al.*²² show that a small-angle parabolic model actually does better than shown here for the Chebyshev-tau model, and that the large-angle parabolic model does better than all of these forward-propagating spectral solutions.

7 DISCUSSION

Forward-propagating wave models for use with conformal mapping have been developed for the angular spectrum, Fourier–Galerkin, and Chebyshev-tau methods. They have been illustrated by application to two problems provided by a simple conformal mapping.

These problems are wave propagation in a diverging channel and in an annular channel.

In Cartesian coordinates, the angular spectrum model, the eigenfunction expansion method (separation of variables), and the Fourier–Galerkin model are identical. In conformal domains, this is not necessarily true. The angular spectrum model is interpreted as an expansion of the velocity potential in terms of the eigenfunctions in the lateral (v) direction. These eigenfunctions are found by separation of variables, eqn (20). For the Fourier–Galerkin method, the lateral eigenfunctions for a channel are a Fourier cosine series, while for the Chebyshev-tau method, the lateral functions are Chebyshev polynomials.

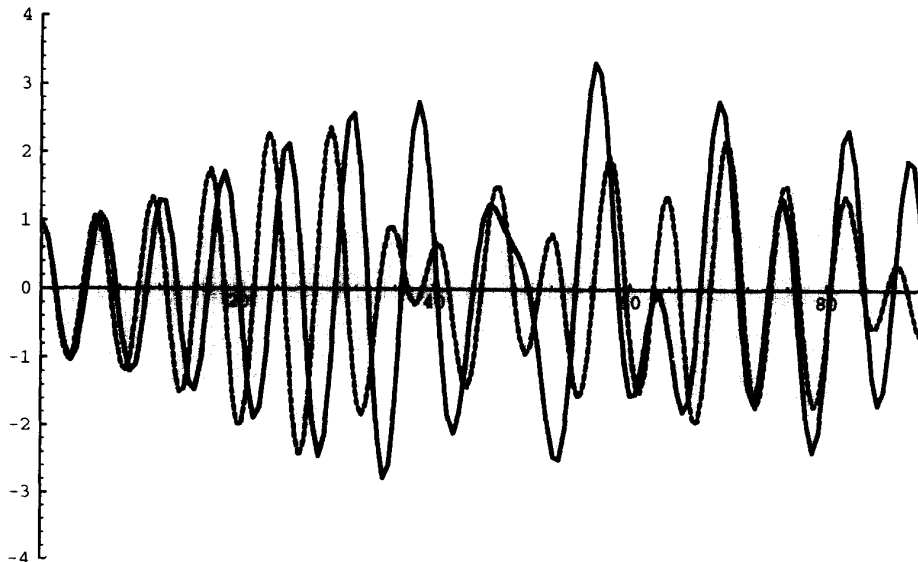


Fig. 14. Comparison of the water surface variation along outer wall between the exact solution (solid line) and the Fourier–Galerkin model (dashed line).

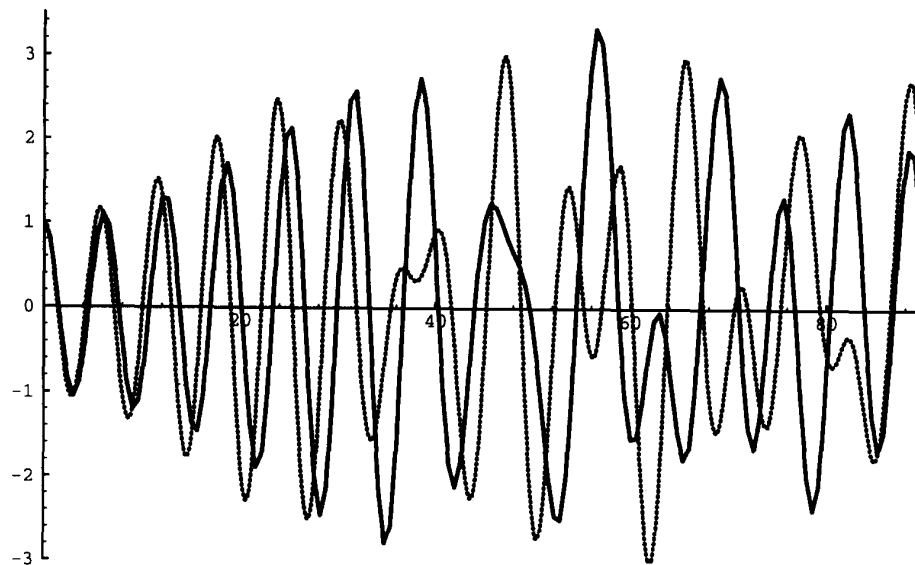


Fig. 15. Comparison of the water surface variation along outer wall between the exact solution (solid line) and the Chebyshev-tau model (dotted line).

For the case of the diverging channel, the lateral eigenfunctions turn out to be cosines; therefore, for this case also, the Fourier–Galerkin method and the angular spectrum method are the same. The Chebyshev-tau method, however, does not approach the exact solution analytically and, numerically, it is not as accurate as the Fourier–Galerkin method.

For the case of an annular channel, the angular spectrum model (using the eigenfunctions given by eqn (27)), coincides with the exact solution, while the Fourier–Galerkin method is shown to become more inaccurate as the channel width increases. The Fourier cosine series differs drastically from the actual lateral eigenfunctions for the wide channel case. This is also true for the Chebyshev-tau forward-propagation model. The source of the errors is the increasing size of ν , which causes the last term in eqn (43) and in eqn (44) to become large. Clearly, the use of the mean value of $k^2 J$ does not properly model the behaviour of the waves for these large ν cases.

Extension of these models to variable depths is relatively simple, as the variable depth case is treated by a variable coefficient Helmholtz equation.²²

ACKNOWLEDGEMENTS

R.A.D. and J.T.K. were supported in part by NOAA Office of Sea Grant, Department of Commerce, under Grant No. NA/16RG0162-03 (Project Nos. R/OE-12 (RAD) and R/OE-13 (JTK)). The US Government is authorized to produce and distribute reprints for governmental purposes, notwithstanding any copyright notation that may appear hereon.

We would like to thank John P. Boyd for helpful comments on the implementation of the Chebyshev approach.

REFERENCES

1. Radder, A. C., On the parabolic equation method for water-wave propagation. *J. Fluid Mech.*, **95** (1979) 159–76.
2. Kirby, J. T. & Dalrymple, R. A., A parabolic equation for the combined refraction–diffraction of Stokes waves by mildly varying topography. *J. Fluid Mech.*, **136** (1983) 453–66.
3. Kirby, J. T. & Dalrymple, R. A., Documentation Manual, Combined Refraction/Diffraction Model, REF/DIF 1, Version 2.4, Center for Applied Coastal Research, Res. Rpt. CACR-92-04, 1992.
4. Stammes, J. J., Løvhaugen, O., Spjelkavik, B., Mei, C. C., Lo, E. & Yue, D. K. P., Nonlinear focusing of surface waves by a lens — theory and experiment. *J. Fluid Mech.*, **135** (1983) 71–94.
5. Dalrymple, R. A. & Greenberg, M. D., Directional wavemakers. In *Physical Modelling in Coastal Engineering*, ed. R. A. Dalrymple. Balkema, Rotterdam, 1984, pp. 67–79.
6. Dalrymple, R. A. & Kirby, J. T., Models for very wide angle water waves and wave diffraction. *J. Fluid Mech.*, **192** (1988) 33–50.
7. Dalrymple, R. A., Suh, K. D., Kirby, J. T. & Chae, J. W., Models for very wide angle water waves and wave diffraction, Part 2. Irregular bathymetry. *J. Fluid Mech.*, **201** (1989) 299–322.
8. Booker, H. G. & Clemmow, P. C., The concept of an angular spectrum of plane waves, and its relation to that of polar diagram and aperture distribution. *Proc. Inst. Elect. Engrs.*, **97** (1950) 11–7.
9. Dalrymple, R. A. & Kirby, J. T., Angular spectrum modelling of water waves. *Rev. Aquat. Sci.*, **6** (1992) 383–404.

10. Suh, K. D., Dalrymple, R. A. & Kirby, J. T., An angular spectrum model for propagation of Stokes waves. *J. Fluid Mech.*, **221** (1990) 205–32.
11. Kirby, J. T., Modelling shoaling directional wave spectra in shallow water. *Proc. 22nd Int. Coastal Engng. Conf.*, ASCE, Delft, 1990, pp. 109–22.
12. Kaihatu, J. M. & Kirby, J. T., Spectral evolution of directional finite amplitude dispersive waves in shallow water. *Proc. 23rd Int. Coastal Engng. Conf.*, ASCE, Venice, 1992, pp. 364–77.
13. Suh, K. D. & Dalrymple, R. A., Application of the angular spectrum model to simulation of irregular wave propagation. *J. Waterway, Port, Coastal & Ocean Engng.*, **119** (1993) 505–19.
14. Boyd, J. P., *Chebyshev and Fourier Spectral Methods*. Springer, Berlin, 1989.
15. Panchang, V. G. & Kopriva, D. A., Solution of two-dimensional water-wave propagation problems by Chebyshev collocation. *Math. Comp. Modelling*, **12** (1989) 625–40.
16. Lanczos, C., *Applied Analysis*. Prentice-Hall, Englewood Cliffs, 1956.
17. Thompson, J. F., *Numerical Grid Generation*. North-Holland, Amsterdam, 1982.
18. Trefethen, L. N. (ed.), *Numerical Conformal Mapping*. North-Holland, Amsterdam, 1986.
19. Liu, P. L.-F. & Boissevain, P. L., Wave propagation between two breakwaters. *J. Waterway, Port, Coastal & Ocean Engng.*, **114** (1988) 237–47.
20. Kirby, J. T., Parabolic wave computations in non-orthogonal coordinate systems. *J. Waterway, Port, Coastal & Ocean Engng.*, **114** (1988) 673–85.
21. Tsay, T.-K., Ebersole, B. A. & Liu, P. L.-F., Numerical modelling of wave propagation using parabolic approximation with a boundary-fitted coordinate system. *Int. J. Num. Methods Engng.*, **27** (1989) 37–55.
22. Kirby, J. T., Dalrymple, R. A. & Kaku, H., Parabolic approximations for water waves in conformal coordinate systems. *Coastal Engng.*, 1994 (in press).
23. Dalrymple, R. A., Water waves past abrupt channel transitions. *Appl. Ocean Res.*, **11** (1989) 170–5.
24. Dalrymple, R. A. & Martin, P. A., Wave diffraction through offshore breakwaters. *J. Waterway, Port, Coastal & Ocean Engng.*, **116** (1990) 727–41.
25. Canuto, C., Hussaini, M. Y., Quarteroni, A. & Zang, T. A., *Spectral Methods in Fluid Dynamics*. Springer, Berlin, 1988.
26. Hoffman, J. D., *Numerical Methods for Engineers and Scientists*. McGraw-Hill, New York, 1992.
27. Buchholz, H., Der Einfluss der Krümmung von rechteckigen Hohlleitern auf das Phasenmass ultrakurzer Wellen. *Elektrische Nachrichtentechnik*, **16** (1939) 73–85.
28. Rostafinski, W., Acoustic systems containing curved duct sections. *J. Acoust. Soc. Am.*, **60** (1976) 23–8.
29. Abramowitz, M. & Stegun, I. A., *Handbook of Mathematical Functions*. Dover, New York, 1965.
30. Kaku, H. & Kirby, J. T., A Parabolic Equation Method in Polar Coordinates for Waves in Harbors. Tech. Rept. UFL/COEL-TR/075, Coastal & Ocean Engng Dept., Univ. Florida, Gainesville, 1988.
31. Martin, P. A. & Dalrymple, R. A., On amphidromic points. *Proc. R. Soc. London Ser. A*, **444** (1994) 91–104.

APPENDIX: CONFORMAL TRANSFORMATION

To determine the governing equation in the transformed domain, the chain rule operators

$$\frac{\partial}{\partial x} = \frac{\partial u}{\partial x} \frac{\partial}{\partial u} + \frac{\partial v}{\partial x} \frac{\partial}{\partial v} \quad \frac{\partial}{\partial y} = \frac{\partial u}{\partial y} \frac{\partial}{\partial u} + \frac{\partial v}{\partial y} \frac{\partial}{\partial v} \quad (\text{A1})$$

are used. Applying these to ϕ for first derivatives, applying them again to obtain the second derivatives, and, finally, substituting into the governing eqn (1) yields

$$(\nabla u)^2 \frac{\partial^2 \phi}{\partial u^2} + 2\nabla u \cdot \nabla v + (\nabla v)^2 \frac{\partial^2 \phi}{\partial v^2} + \frac{\partial \phi}{\partial u} \nabla^2 u + \frac{\partial \phi}{\partial v} \nabla^2 v + k^2 \phi = 0 \quad (\text{A2})$$

While the derivatives of ϕ in this equation are taken with respect to the mapped coordinates, the coefficients still involve derivatives of u and v with respect to x and y . Applying both operators eqn (A1) to dx , we obtain

$$1 = \frac{\partial u}{\partial x} \frac{\partial x}{\partial u} + \frac{\partial v}{\partial x} \frac{\partial x}{\partial v} \quad \text{and} \quad 0 = \frac{\partial u}{\partial x} \frac{\partial y}{\partial u} + \frac{\partial v}{\partial x} \frac{\partial y}{\partial v}$$

This pair of equations can be easily solved to give

$$\frac{\partial u}{\partial x} = \frac{1}{J} \frac{\partial y}{\partial v} \quad (\text{A3})$$

$$\frac{\partial v}{\partial x} = \frac{1}{J} \frac{\partial y}{\partial u} \quad (\text{A4})$$

where J is the Jacobian, defined by eqn (18). The same procedure is repeated for dy , resulting in

$$\frac{\partial u}{\partial y} = -\frac{1}{J} \frac{\partial x}{\partial v} \quad (\text{A5})$$

$$\frac{\partial v}{\partial y} = \frac{1}{J} \frac{\partial x}{\partial u} \quad (\text{A6})$$

For a conformal mapping, the Cauchy–Riemann conditions are required to ensure that the transformation is holomorphic (that is, derivatives exist everywhere). These are

$$\frac{\partial u}{\partial x} = \frac{\partial v}{\partial y} \quad \text{and} \quad \frac{\partial u}{\partial y} = -\frac{\partial v}{\partial x}$$

By taking derivatives of these expressions, it is straightforward to show that $\nabla^2 u = 0$ and $\nabla^2 v = 0$. Furthermore, by substituting from eqns (A4) and (A6), the Cauchy–Riemann conditions show that

$$\frac{\partial x}{\partial u} = \frac{\partial y}{\partial v} \quad \text{and} \quad \frac{\partial x}{\partial v} = -\frac{\partial y}{\partial u}$$

Utilizing the last two sets of conditions, the general curvilinear coordinate system governing equation (A2) is greatly simplified to one valid for conformal coordinate systems: the result is eqn (17).